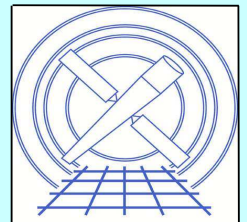


Error Analysis of HRC-I ECF Regions Applied to ACIS Data

Eli Beckerman, Diab Jerius

Smithsonian Astrophysical Observatory
60 Garden Street, Cambridge, MA 02138



Abstract

In order to determine the errors associated with using HRC-I enclosed count fraction (ECF) tables on ACIS data, we raytrace a grid of off-axis observations with both HRC-I and ACIS-I at the airpoint. We use two different approaches to determine the impact of using HRC-I ECFs on ACIS data. First, we compare the radii at which specific enclosed count fractions are reached on HRC and on ACIS. Second, we apply the HRC ECF regions to ACIS data and study the relative enclosed count fractions at those radii. We find that the radii of the 50% ECFs differ by as much as 43% between the detectors, while the radii of the 90% ECFs differ by a maximum of 24%. When applying the HRC ECF regions to ACIS data, we see a maximum error of 35% with the 50% ECFs and only 6.2% for the 90% ECFs.

Introduction

The enclosed count fraction (ECF) tables which have been released to the public were generated via *SAOsc* raytraces using an infinite HRC-I as the detector. We examine the errors associated with using these HRC-I ECFs to characterize the PSF of ACIS observations. In particular, we concentrate on the effect of projecting to the different detector planes. We ignore the difference between the pixel sizes by not pixelizing the data after it is projected to the detector surface.

We raytrace observations with the HRC-I and ACIS-I at the airpoint, at positions that make up a polar grid on the ACIS-I as well as a line across the middle of the ACIS-S. In addition to comparing the HRC and ACIS ECFs directly, we also apply the HRC ECF regions to the ACIS simulations.

This study utilizes circular regions created by the CXC Optics group's circular ECF program, *enen-evts*.

Setup

We choose a grid of positions to raytrace such that the far ACIS-S chips would be covered with ACIS-I at the airpoint. Figure 1 below shows this grid against the ACIS detectors. The sources that fall on ACIS-S are spaced 2 arcminutes apart.

We raytrace a point source with a spectrum such that there will be uniform signal-to-noise across the entire spectrum. We determined that a high ray density was necessary because the enclosed count fractions were sensitive to the number of source counts. Each raytrace has about 10^6 total counts.

We then project the rays to the focal plane with the CXC Optics group's detector model, *detcpl*. We use non-pixelized detector coordinates for ECF generation, which apart from the effects of dither and aspect reconstruction are functionally identical to the sky coordinates that users see. The simulations are split into 1 keV energy bins from 0-8 keV to exhibit the energy dependence of the errors.

A number of complicating factors are handled as follows:

- We use an infinite detector plane to avoid chip gaps.
- We don't treat the impacts of pixelization or telescope dither.
- Ghost rays are filtered out, though they may affect real observations at off-axis angles $> 15^\circ$. Their large spatial extent dramatically inflates the outer annuli. Real observations will typically not be affected by them because of their low surface brightness. However, as our simulations do not include background contamination they significantly bias our results and must be excluded to match on-orbit performance.

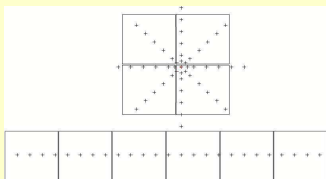


Figure 1. Positions of raytraces on ACIS, with ACIS-I at the airpoint. These positions were chosen to sample different parts of the I array as well as the far chips of the S array.

Analysis

We compare the HRC-I and ACIS-I ECFs in two manners. First, we derive the ratios of the radii for the 50%, 90%, and 95% ECFs for both detectors. This provides an indication of how the difference in detector planes distorts the shape of the PSF. In the second comparison, which is more useful for observers, we apply the ECF regions derived from the HRC-I simulations to the ACIS-I simulations and measure the actual count fractions found in those regions. The two comparisons are shown for the 90% ECFs as a function of energy for the $\phi=0$ ACIS-I subset in Figure 2. The plot on the left is the ratio of 90% ECF radii between ACIS and HRC, while the one on the right is the ratio of enclosed count fractions at the HRC 90% ECF radii. Qualitatively the results at the other azimuthal angles are similar to those at $\phi=0$, but there is a noticeable azimuthal effect on the errors.

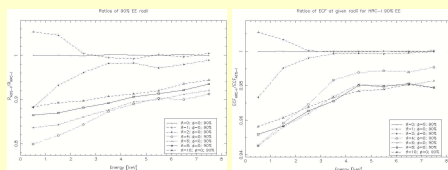


Figure 2. Left: Ratio of the 90% ECF radii on ACIS and HRC, which is a direct comparison of the ECF regions. Right: Ratio of the enclosed count fractions between ACIS and HRC at the 90% HRC ECF radii, which indicates the errors associated with applying the HRC ECF tables to ACIS data and is more useful for observers.

For further off-axis results we focus on the 90% ECFs. Since the underlying model of the optics does not perform as well off-axis as it does on-axis, especially in the core of the PSF, the 50% ECFs are not reliable off-axis. Figure 3 below shows results for the 50% and 95% ECFs at $\phi=0$ as an example. Comparing to the 90% ECFs in Figure 2, it is clear that the errors for the 50% ECFs are larger and those for the 95% ECFs are smaller.

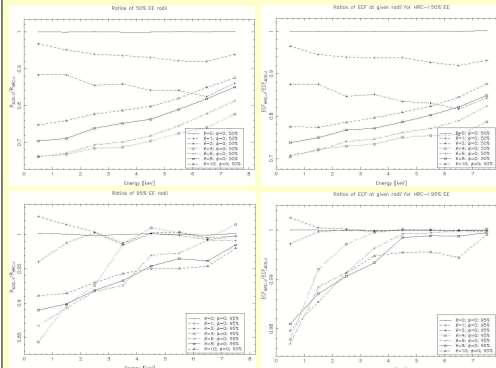


Figure 3. Left: Ratios of the 50% and 95% ECF radii on ACIS and HRC. The 50% radii differ by as much as 34%. Right: Ratios of enclosed count fractions at the 50% and 95% HRC ECF radii. The maximum error is about 30%.

Figure 4, below, shows the results for the raytraces that fall on the ACIS-S array, using only the 90% ECFs. Again, the plots on the left are the ratio of the ECF radii, and those on the right are the ratio of the enclosed count fractions at the HRC 90% radii. Figure 5, at the bottom of this panel, shows the results where we find the maximum errors.

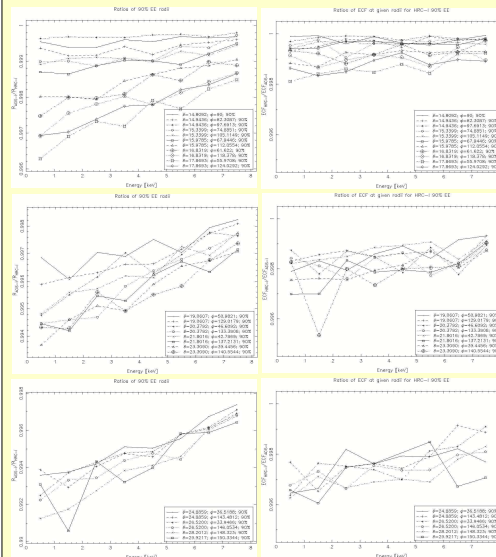


Figure 4. Ratios of 90% ECF radii (left) and ECF at 90% HRC radii (right) for 14 $\phi < 30^\circ$. These ratios, for which the ACIS simulations fall on the S-array, are closer to 1 than those in Figure 2, despite being further off-axis.

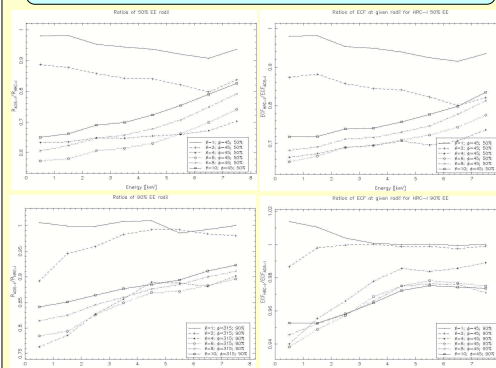


Figure 5. The 50% and 90% ratios of ECF radii (left) with the largest errors. The maximum errors in radii are 43% for the 50% ECFs and 24% for the 90% ECFs. On the right are the ratios of enclosed count fractions at the 50% and 90% HRC ECF radii. These are the applied errors, and we see maximum errors of 35% for the 50% radii and 6.2% for the 90% radii.

From Figure 5, we find that errors in the ECF radii of up to 43% are possible when looking at the 50% enclosed count fractions. Actually applying the HRC-I regions to the ACIS data could lead to errors of up to 35%. The largest errors are seen in the 0-1 keV range for off-axis angles of 4-6°. Looking at the 90% ECF regions, the radii disagree by a maximum of 24%, and applying them to ACIS data would result in a maximum error of 6.2%.

Interestingly, the largest errors are seen at relatively small off-axis angles (4-6°). On-axis, of course, both the HRC and ACIS PSFs agree perfectly. But as we move further off-axis, and eventually onto the S-array, the ratios begin to approach unity.

To understand this, we examine the geometries of the detectors and the focal surfaces for different energies and off-axis angles. Figure 6 shows the focal surface for 3 different energies (1,4,8 keV) as a function of θ (at an azimuthal angle of $\phi=0$). The HRC-I and ACIS-I detector planes are included for comparison. The most significant indicator of the PSF differences turns out to be the distance between the focal surface and the detector plane for each raytrace. We compare these distances for the HRC and ACIS data in Figure 7, by taking their ratio. We also plot the distances between the HRC and ACIS detectors in Figure 8. Note that these are functions of azimuth, so that, for instance, at $\phi=45^\circ$ the distance between the planes is larger.

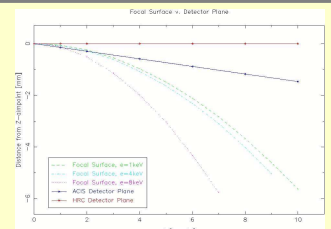


Figure 6. Comparisons of the focal surfaces and the detector planes of HRC-I and ACIS-I, at energies of 1,4, and 8 keV, as a function of off-axis angle θ .

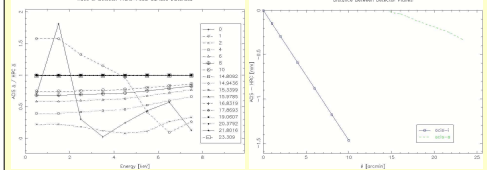


Figure 7. Left: ACIS/HRC Ratio of detector plane - focal surface distances. Right: Distance between HRC and ACIS detector planes, as a function of off-axis angle θ .

There are only a few instances where the PSF on the HRC is tighter than that on ACIS, resulting in a ratio of the ACIS/HRC 90% ECF radii to be greater than 1. This is mainly at low energies and an off-axis angle of $\theta=1$. Looking at the e-1 keV focal surface in Figure 6, it is evident that it is closer to the HRC detector at $\theta=1$. This also shows up in the ratio of the focal surface - detector plane distances in Figure 7, where it is greater than 1 for $\theta=1$ at low energies. The other ratio greater than 1 in that plot is the ratio of very small numbers for $\theta=1$.

At large off-axis angles, the distance between the two detector planes is so much smaller than the distance between the detector plane and the focal surface, so the results in Figure 4 ($\theta=14$) are closer to unity than those in Figure 2 ($\theta=10$). The other effect is that the latter simulations fall on ACIS-I, while the far off-axis simulations are on ACIS-S. Figure 7 shows that the ACIS-I chips are more steeply tilted, and so the distance between ACIS-I and HRC-I can be greater than that between the ACIS-S and HRC-I.

The energy dependence of the errors, as seen in Figures 2-5, can be explained by the change in the shape of the focal surface with energy, as in Figure 6. The focal surface gets much steeper at higher energies, and this has the same effect as going to larger off-axis angles -- the HRC and ACIS results are more similar because the distance between their detector planes is so much smaller than their distance from the focal surface.

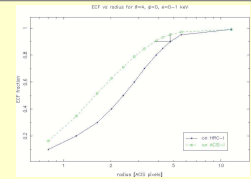


Figure 8. Plot of HRC and ACIS enclosed count fraction vs. radius for $\phi=0, \phi=1, \phi=10$ 1 keV. This demonstrates how the errors in the radii are more significant than the errors in the enclosed counts.

Conclusion

This study compares the PSF projected to the HRC and ACIS focal planes in order to determine the errors associated with using HRC ECF regions to characterize the ACIS PSF. It is done without pixels, detector edges, ghost rays, or dither. We find that the 50% HRC ECF regions are not very suitable for applying to off-axis ACIS data, resulting in errors of up to 35%. The 90% radii themselves differ by as much as 43%. We recommend using the 90% HRC ECF regions, whose radii differ from the ACIS regions by as much as 24%, but result in a maximum error of 6.2% between 4-6° off-axis. These quoted errors, it should be noted, are not representative but rather worst-case errors.

The errors in the radii are much larger than those in the enclosed fractions, which may seem inconsistent. In fact they are not, as is indicated by Figure 8, which shows the ECF versus radius for both the HRC and ACIS data. Moving from the HRC data to the ACIS data, and starting at the 90% HRC ECF radius, the change in radius is far bigger than the change in the enclosed count fraction.

At large off-axis angles, the differences between the HRC and ACIS detectors are negligible.